Supplemental Information

C.M. Moir[1,2], Scott C. Riggs[2], J.A. Galvis[2], X. Lian[1,2], P. Giraldo-Gallo[2], Jiun-Haw Chu[3], P. Walmsley[4], Ian R. Fisher[4,5], Arkady Shekhter[2] and G.S. Boebinger[1,2]

[1]Florida State University, Tallahassee, FL 32306, USA
[2]National High Magnetic Field Laboratory, Florida State University, Tallahassee, FL 32310, USA
[3]University of Washington, Seattle, WA 98195, USA
[4]Stanford University, Stanford, CA 94305, USA
[5]SLAC National Accelerator Laboratory, Menlo Park, CA 94025, USA

1 Samples and Methods

Single crystals of $BaFe_2(As_{1-x}P_x)_2$ were grown from FeAs flux at Stanford University as described elsewhere [1]. The single crystals used in this study measured approximately 0.4 mm × 0.5 mm × 0.04 mm. Doping values were determined by magnetization measurement determination of T_c. Single crystals were measured in a VSM SQUID with an applied field of 20 Oe . Zero-field cooled superconducting transitions were typically less than 3.5 K in width. The temperature at which the moment was 2% of the maximum magnetic moment was taken as the T_c [Supplementary Figure 1]. The doping of each sample was determined by comparing the measured T_c to the aggregated T_c versus doping from Refs [1–5]. The resulting curve and the doping values of the samples measured in the current work are shown in Figure 2a of the main text. Sample quality is discussed further in SI Section 5.

The specific heat calorimeter platform is sapphire with a NiChrome heater and Cernox 10-30 wafer thermometer deposited directly on the sapphire. The calorimeter thermometer was magnetic field calibrated up to 40 T over the temperature range 1.4 K to 12 K. Calibration accuracy was confirmed by the measurement of a high purity, thin copper plate with a mass of 1.6 mg at both zero-field and 15T.

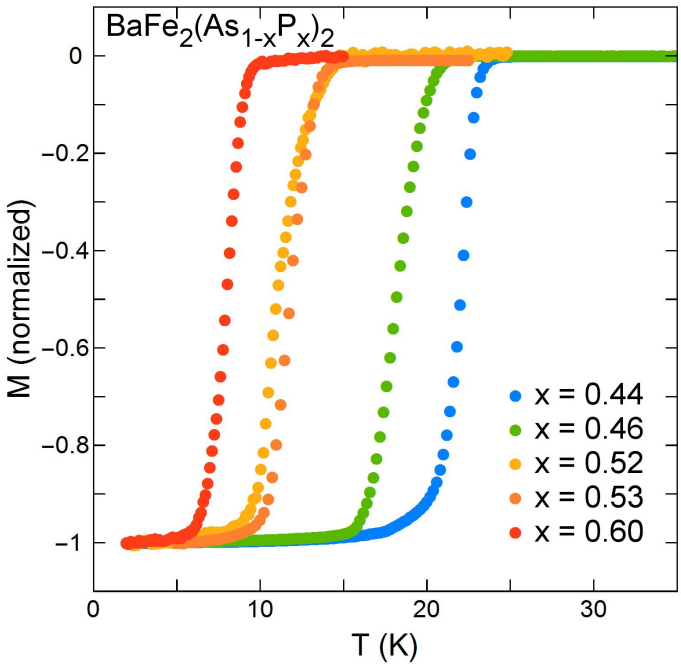

Figure 1: Normalized zero-field-cooled magnetization data for $0.44 \leq x \leq 0.60$. Samples were measured in a Quantum Design VSM SQUID with an applied field of 20 Oe. Transition widths were determined from 5% to 95% of the magnetic moment at the lowest temperature, and found to be less than 3.5 K for $0.46 \leq x$. At $x = 0.44$ the transition width is 4.1 K.

Specific heat measurements were performed on a mosaic of several crystals with an aggregate mass of 0.2 mg $\leq$ m $\leq$ 1 mg. Samples were attached to the center of the sapphire platform of the calorimeter with a thin layer of Apiezon N-grease in a mosaic formation such that the c-axes of the single crystals were parallel to the applied magnetic field.

2 Phenomenology of Nodal Superconductivity

The magnetic field dependence of C/T below the saturation regime was interpreted using Volovik's phenomenology of nodal superconductivity [6]. At fields such that $(T/T_c)^2 \ll H/H_{c2} \ll 1$, the behavior of C/T is $\sqrt{H}$. In the opposite limit $H/H_{c2} \ll (T/T_c)^2$ the behavior of C/T is linear in field, which is qualitatively con-

sistent with the parabolic tails at the very low fields in the $\sqrt{H}$ plots of Figures 1b and 2b of the main text.

At small T/T_c the crossover from $\sqrt{H}$ behavior to saturation of C/T in field is sharp. As T/T_c increases, a 'hump' feature at the crossover to saturation develops for reasons that are yet not understood. At sufficiently high temperature, the hump and the low field 'tail' overlap and the resulting superposition gives the false impression of a $\sqrt{H}$ dependence. This 'false $\sqrt{H}$' behavior can be distinguished from Volovik $\sqrt{H}$ behavior by examining the evolution of the slope of the $\sqrt{H}$ dependence with temperature. The phenomenology of nodal superconductors indicates that the slope of $\sqrt{H}$ is inversely proportional to H_{c2}. As temperature increases, H_{c2} decreases, and therefore the slope of Volovik $\sqrt{H}$ behavior must also increase. By imposing this requirement on our data, we create an upper temperature limit for each doping above which γ_H cannot be determined. All data presented in the main text were taken at temperatures below this limiting temperature.

As stated above, the reason for the 'hump' feature is not yet understood. Note, however, that there is no reason why the two limiting behaviors we observe in Figure 2 of the manuscript should precisely meet at the same value of specific heat when the sample transitions to the normal state. In particular, the low field $\sqrt{H}$ behavior has a slope that, in the Volovik picture, is dictated by the physics of the quasiparticles that are Doppler shifted around the vortices in the mixed state. By contrast, the high-field saturated value of the specific heat is dictated by the normal state density of states. There is no reason a priori that the two behaviors should meet at a point. Thus, for $x = 0.52, 0.53$, and 0.60, the $\sqrt{H}$ in the vortex state appears to "overshoot" the normal state density of states. The existence of this "overshoot" requires a crossover regime in which the specific heat settles to the high-field normal state value.

3 Comparison of Current Work to Previous Quantum Oscillation Studies

Supplemental Figure 2c shows that the equivalent mass associated with γ_H (blue circles) is enhanced by about 110%, whereas the mass determined by quantum oscillation measurements (open black squares) over the same doping range increases by only about 40% for a single electron pocket (denoted the β-pocket) [2, 4]. The equivalent mass associated with γ_H inherently accounts for all pockets that open a superconducting gap below the superconducting temperature, whereas the quantum oscillations in overdoped $BaFe_2(As_{1-x}P_x)_2$ only determine doping evolution of the mass of a single electron pocket (β) [2, 4]. It is plausible that pockets for which a

quantum oscillation mass is not resolved by these measurements over a broad doping range have stronger mass enhancement, thus accounting for this difference. Our data therefore suggest that some pockets must have an even stronger mass enhancement than that reported for the β-pocket.

Supplemental Figures 2a and 2b contain the doping dependence of γ_H and γ_{bg}, respectively. As stated in the main text, γ_{bg} is both magnetic field independent and temperature independent over the entire range of measured fields ($0 < \mathrm{H} < 35$ T) and temperatures ($\sim 1.5\ \mathrm{K} < \mathrm{T} < 20$ K). This indicates that γ_{bg} does not arise from pair-breaking, as that would imply both temperature and magnetic field dependence over our broad experimental regime. Additionally, γ_{bg} increases with doping which is consistent with the residual γ observed in $\mathrm{Ba(Fe_{1-x}Co_xAs_2}$ and concluded not to arise from pair breaking [7]. If γ_{bg} arises from one or more Fermi pockets, they must be Fermi pockets that do not superconduct. More strictly speaking, given that our data are at finite temperature such that we must extrapolate from our $\sqrt{H}$ behavior observed down to $\sim$1 T, these must be Fermi pockets that, if superconducting, are so weakly superconducting that they superconduct at temperatures below ~ 1.5 K or their superconductivity is destroyed by magnetic fields of $\sim$1 T even at our lowest experimental temperatures. Thus, γ_H *by itself* represents the electronic specific heat of the robustly superconducting Fermi pockets.

Assuming a 2D Fermi surface with an unwarped, cylindrical pocket and parabolic energy dispersion, the average electronic energy at constant volume of the sample is given by

$$\bar{\mathrm{E}} = \bar{\mathrm{E}}_0 + \frac{\pi^2}{3} {k_B}^2 T^2 \frac{m^* A}{2\pi\hbar^2}$$

where A is the area of the unit cell in the Fe-As plane (i.e. a-b plane), m^* is the quasiparticle mass. We therefore define an effective quasiparticle mass m with units of m_e (i.e. $m = m^*/m_e$). Taking the derivative of $\bar{\mathrm{E}}$ with respect to temperature, we obtain the electronic specific heat per formula unit

$$\mathrm{C} = \frac{\pi A m m_e k_B T}{3\hbar^2} N_A$$

from which we can determine an effective quasiparticle mass. For a Fermi surface with multiple pockets, the total electronic specific heat is the sum of the contributions from each pocket.

Thus, a conversion from the electronic specific heat to effective mass depends only on the area of the unit cell. Neutron diffraction studies on $\mathrm{BaFe_2(As_{1-x}P_x)_2}$ at low temperatures have reported the lattice parameters and unit cell volume with doping across the superconducting dome [8]. Using these lattice parameters, at

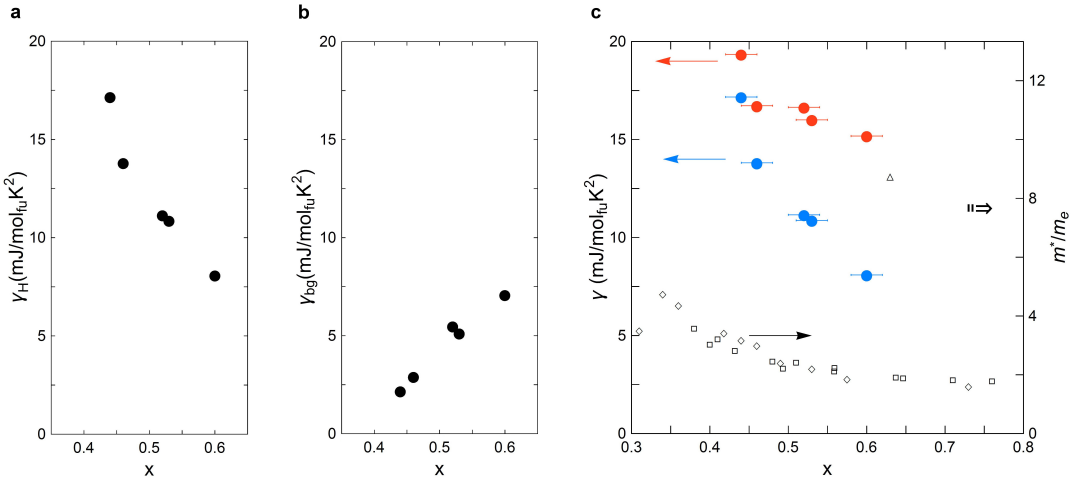

Figure 2: a. Doping dependence of γ_H. **b**. Doping dependence of γ_{bg}. **c**. Doping dependence of γ_H (blue circles), γ_{total} (red circles), and effective masses reproduced from previous quantum oscillation studies. Empty black squares represent the effective mass of the β-pocket [2], the empty triangle and arrow indicate the sum of the effective masses for all observed pockets at dopings $x = 0.63$ [3] and $x = 1$ [9], and empty diamonds indicate effective masses determined from transport measurements using the Kadowaki-Woods ratio [1].

$x = 0.35$, C $= 1.5$mJ/molK$^2 \times \sum m^*/m_e$, where the sum is over all pockets in the Fermi surface. For the doping range studied in the current work, the a-b planar area of the unit cell changes less than 0.2 Å^2 which corresponds to a difference in the specific-heat-to-effective-mass-conversion factor of less than 2%. Therefore a specific-heat-to-effective-mass-conversion factor of 1.5 was used for all dopings.

The extension of such a sum to the case where pockets have insignificant warping is straightforward. However, angle-dependent quantum oscillation studies have shown that the $BaFe_2(As_{1-x}P_x)_2$ pockets experience measurable warping [2]. For those pockets, we take the arithmetic mean of the maximum and minimum masses reported in previous quantum oscillation studies [2, 3].

We now consider the absolute value of the γ_H equivalent mass. The total mass of all pockets from quantum oscillation measurements at $x = 0.63$ (triangle) [3] and in the parent compound ($x = 1$) (arrow) [9] are also shown in Supplemental Figure 2c. Both are dramatically higher than the equivalent quasiparticle mass deduced from γ_H at our highest doping, $x = 0.60$. We note that $\gamma_{total} = \gamma_H + \gamma_{bg}$ (red

circles) matches better the quantum oscillation data available for the total mass of all pockets. This may suggest that $\gamma_{\rm total}$ corresponds to the Fermi surface density of states of all pockets. Such interpretation implies that γ_{bg} corresponds to the density of states of a non-superconducting pocket or pockets. Since γ_{bg} decreases approaching optimal doping (Supp. Fig. 2b), such a non-superconducting pocket would experience a mass decrease by a factor two in the same doping range over which the superconducting pockets double their mass.

4 Comparison of Current work to Previous Specific Heat Studies

Previous studies that have investigated the specific heat of $BaFe_2(As_{1-x}P_x)_2$ as a function of doping have focused on the jump in specific heat at T_c in order to estimate the normal state density of states. This strategy necessarily depends on assumptions concerning the behavior of phonons over a large temperature range, as well as the modeling of the jump in C/T_c and the universal applicability of the BCS ratio, $C/T_c\gamma_n = 1.43$. From the current work, we have a direct measurement of the normal-state specific heat once superconductivity is suppressed by magnetic field, from which the ratio $C/T_c\gamma_n$ can be experimentally determined.

In order to build a bridge between our high-magnetic field method and previous jump-at-T_c methods, we replicated previous studies for three dopings using the same samples measured in the current work. To remove the contribution to the specific heat from phonons, we measured the zero-field specific heat and subtracted a second order polynomial as a function of T^2 fitted above T_c. Due to the small temperature range over which fitting was performed, the uncertainty in the fitting parameters was constrained by imposing entropy conservation from $0 \leq T \leq T_c$. The resulting curves are shown in Supplementary Figure 3. The height of the jump in the specific heat was determined by further constraining that entropy be conserved through the superconducting transition anomaly.

We determine an upper bound to our superconducting transition width by calculating the distance from the beginning of the upturn above T_c to the apex of the specific heat peak in the raw data. This corresponds to a maximum transition width of 3 K, comparable to the transition widths determined by the same method in Refs [10–12], although sharper transitions, 1.5 K in width, were measured in Ref [2]. We also note that the width of the transition decreases with increasing doping for our samples. Our observed transition widths correspond to a $\sim$0.04 spread in P doping on the As site, which yields a 1% uncertainty in the molar mass, resulting in a 1%

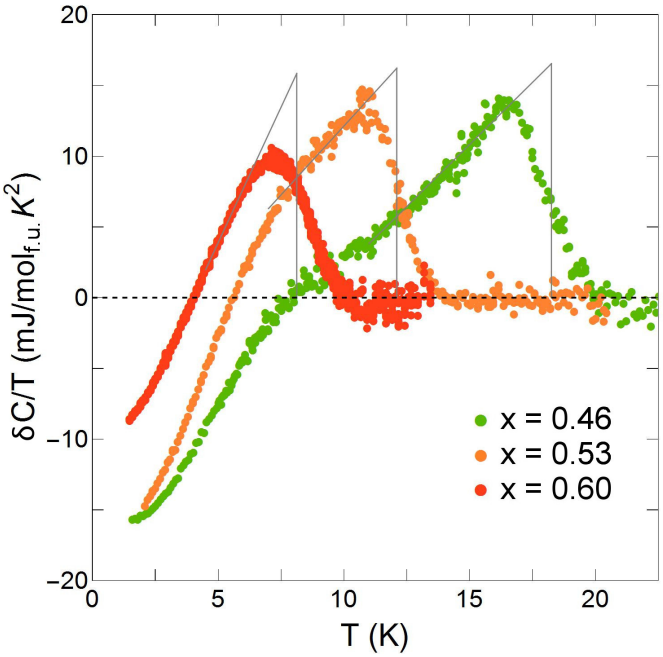

Figure 3: Doping dependence of the jump in the electronic specific heat at zero-field, plotted as the deviation of the electronic specific heat from its high temperature value. The height of the electronic specific heat jump is only weakly dependent on doping with no evidence of parabolic or cubic dependence on T_c [13, 14]. The magnitude of the jump at $x = 0.46$ is much smaller than that reported by previous studies [2, 10], however, the shape of the transition is similar to those reported in nano-calorimeter studies [10], and the height of the jump at $x = 0.53$ is comparable to that shown in Ref. [10] for $x = 0.55$.

uncertainty in the specific heat per mole over each mosaic of crystals at the three nominal dopings measured. Figure 3 of the main text and Supplemental Figure 2c includes error bars from these doping uncertainties.

We see little change in the magnitude of the jump in C/T at T_c with doping over the measured doping range; however, the range of T_c for samples in this work is too narrow to make any reliable conclusion about possible scaling of the jump with T_c [7,8]. The ratio $C/T_c\gamma_n$ can be calculated using either γ_H or γ_{total} as the normal state electronic specific heat [See Supplemental Figure 4]. Two disparate behaviors are apparent: a constant value of the ratio with a magnitude close to 1, and a ratio that increases from $\sim$1 to $\sim$2 for the three samples studied. Neither of

these behaviors is consistent with BCS theory in the weak coupling limit.

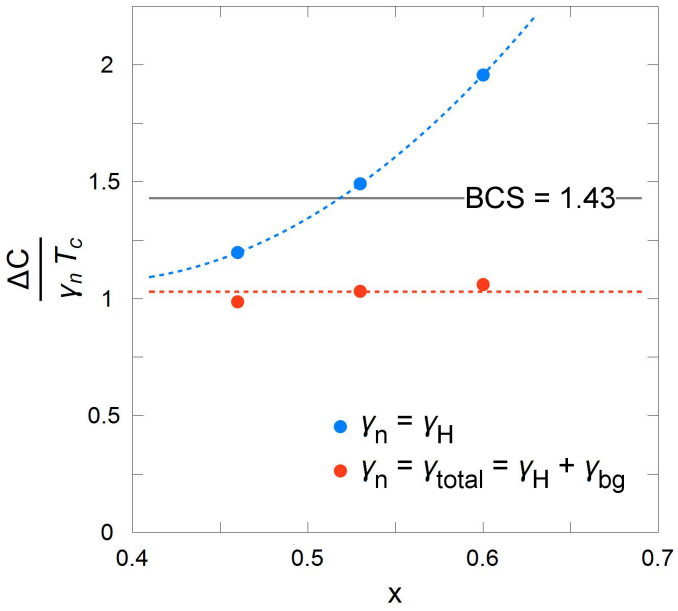

Figure 4: The BCS ratio, $C/T_c\gamma_n$, as a function of doping. Gray line is the BCS value 1.43. Dashed colored lines are guides for the eye.

5 Sample Quality

In our measurements, we observe a zero-field, zero-temperature electronic specific heat, γ_{bg}, which is finite and increases with increasing doping, such that at $x = 0.60$ the magnitude of γ_{bg} is nearly equal to the value of γ_H [Supplemental Figure 2a,b]. We make no *a priori* assumptions concerning the origin of γ_{bg}, and therefore must consider the possibility that γ_{bg} arises from disorder, such as flux inclusions or impurities, in the samples rather than from the Fermi surface or more exotic physics.

Both specific heat and magnetization transitions show at most a ∼3.5 K width of the transition into the superconducting state for $0.46 \leq x$. This width is comparable with the superconducting transitions in specific heat on single crystals as reported in a number of studies [10–12], although narrower widths (1.5 K) have been reported in Ref [2]. As stated in SI Section 4, the widths in T_c as seen in the jump in the specific heat at T_c translate a ∼1% uncertainty in the values of γ. This would imply

that doping inhomogeneity within a single crystal and across the mosaic of samples is unlikely to be the source of γ_{bg}. Additionally, we observed in SI Section 4 that the width of the specific heat jump at T_c decreases with increasing doping. One would expect the opposite trend if γ_{bg} arose from doping inhomogeneity that affects T_c. It is worth noting that γ_{bg} increases by a factor of five from $x = 0.46$ to $x = 0.60$.

Microprobe studies performed on 2-4 crystals at doping $x = 0.3$, 0.44, and 0.60 show an increase in the number of flux inclusions with increasing doping. If flux inclusions are responsible for the observed γ_{bg}, we would not expect the flux and the superconducting sample to have the same density of states, i.e. one could not simply add γ_{bg} to γ_H to yield a meaningful γ_{total}. However, as shown in Supplemental Figure 2, γ_{total} agrees well with the sum of the effective quasiparticle masses determined by quantum oscillation measurements. Because quantum oscillations are only sensitive to quasiparticles at the Fermi surface, this suggests thatγ_{total}, and therefore γ_{bg}, originate from Fermi surface quasiparticles. Such a conclusion implies that γ_{bg} arises from non-superconducting pockets. However, the claim of non-superconducting pockets would be at odds with ARPES measurements that report comparable superconducting gap energies for all pockets on the Fermi surface [15].

The observed doping dependence of γ_{bg} might alternatively suggest a non-Fermi surface origin of that component of the specific heat, arising perhaps from localized electrons. However, quantum oscillation measurements probe the Fermi surface and would not detect these localized electrons. A final possibility is that γ_{bg} arises from non-Fermionic modes associated with quantum criticality [16, 17], although an interpretation in terms of specific heat is not straightforward. We emphasize that these questions can now be discussed based on a model-independent analysis of magnetic-field-dependent specific heat as presented in this work. In particular, our measurement may renew an interest in the evolution of the specific heat jump at T_c and its relation to the electronic density of state in high temperature superconductors.

6 References

[1] Analytis, J. G. *et al.* Transport near a quantum critical point in $BaFe_2(As_{1-x}P_x)_2$ *Nature Physics* **10**, 194-197 (2014).

[2] Walmsley, P. *et al.* Quasiparticle mass enhancement close to the Quantum Critical Point*Phys. Rev. Lett.* **110**, 257002 (2013).

[3] Analytis, J. G., Chu, J.-H., McDonald, R.D., Riggs, S.C. & Fisher, I.R. Enhanced Fermi-surface nesting in superconducting $BaFe_2(As_{1-x}P_x)_2$ revealed by the de Haas-van Alphen effect *Phys. Rev. Lett.* **105**, 207004 (2010).

[4] Shishido, H. *et al.* Evolution of the Fermi surface of $BaFe_2(As_{1-x}P_x)_2$ on entering the superconducting dome *Phys. Rev. Lett.* **104**, 057008 (2010).

[5] Nakajima, M. *et al.* Growth of $BaFe_2(As_{1-x}P_x)_2$ single crystals ($0 \leq x \leq 1$) by Ba_2As_3/Ba_2P_3-flux method *J. Phys. Soc. Jpn.* **81**, 104710 (2012).

[6] Volovik, G.E. Superconductivity with lines of GAP nodes: density of states in the vortex *Pis'ma Zh. Eksp. Teor. Fiz.* **58**, 457-461 (1993).

[7] Hardy, F. *et al.* Doping evolution of superconducting gaps and electronic densities of states in $Ba(Fe_{1-x}Co_x)_2As_2$ iron pnictides *EPL* **91**, 47008 (2010).

[8] Allred, J. M. *et al.* Coincident structural an magnetic order in $BaFe_2(As_{1-x}P_x)_2$ revealed by high-resolution neutron diffraction *Phys. Rev. B* **90**, 104513 (2014).

[9] Arnold, B. J. *et al.* Nesting of electron and hole Fermi surfaces in nonsuperconducting $BaFe_2(As_{1-x}P_x)_2$ *Phys. Rev. B* **83**, 220504(R) (2011).

[10] Diao, Z. *et al.* Microscopic parameters from high-resolution specific heat measurements on superoptimally substituted $BaFe_2(As_{1-x}P_x)_2$ single crystals *Phys. Rev. B* **93**, 014509 (2016).

[11] Bohmer, A.E. *et al.* Nematic susceptibility of hole-doped and electron-doped $BaFe_2As_2$ iron-based superconductor from shear modulus measurements *Phys. Rev. B* **112**, 047001 (2014).

[12] Campanini, A. *et al.* Superconducting gap evolution in overdoped $BaFe_2(As_{1-x}P_x)_2$ single crystals through nanocalorimetry *Rep. Prog. Phys.* **91**, 245142 (2015).

[13] Zaanen, J. Specific-heat jump at the superconducting transition and the quantum critical nature of the normal state of pnictide superconductors *Phys. Rev. B* **80**, 212502 (2009).

[14] Bud'ko, Sergey L., Ni, N., & Canfield, P. C. Jump in specific heat at the superconducting transition temperature in $Ba(Fe_{1-x}Co_x)_2As_2$ and $Ba(Fe_{1-x}Ni_x)_2As_2$ single crystals *Phys. Rev. B* **79**, 220516(R) (2009).

[15] Zhang, Y. *et al.* Nodal superconducting-gap structure in ferropnictide superconductor $BaFe_2(As_{0.7}P_0.3)_2$ *Nature Physics* **8**, 371–375 (2012).

[16] Oganesyan, V., Kivelson, S.A. & Fradkin, E. Quantum theory of a nematic Fermi fluid *Phys. Rev. B* **64**, 195109 (2001).

[17] Kogan, V.G. Strong pairbreaking in anisotropic superconductors *Phys. Rev. B* **81**, 184528 (2010).